Modeling Pilot Pulse Control

Edward Bachelder
San Jose State University
U.S. Army Aviation Development Directorate
Moffett Field, California 94035

Ronald Hess
University of California, Davis
Mechanical & Aerospace Engineering
Davis, California 95616

Martine Godfroy-Cooper
San Jose State University
NASA Ames Research Center
Moffett Field, California 94035

Bimal Aponso
NASA Ames Research Center
Moffett Field, California 94035

Abstract. In this study, behavioral models are developed that closely reproduced pulsive control response of two pilots from the experimental pool using markedly different control techniques (styles) while conducting a tracking task. An intriguing find was that the pilots appeared to: 1) produce a continuous, internally-generated stick signal that they integrated in time; 2) integrate the actual stick position; and 3) compare the two integrations to issue and cease pulse commands. This suggests that the pilots utilized kinesthetic feedback in order to perceive and integrate stick position, supporting the hypothesis that pilots can access and employ the proprioceptive inner feedback loop proposed by Hess' pilot Structural Model [1]. The Pulse Models used in conjunction with the pilot Structural Model closely recreated the pilot data both in the frequency and time domains during closed-loop simulation. This indicates that for the range of tasks and control styles encountered, the models captured the fundamental mechanisms governing pulsive and control processes. The pilot Pulse Models give important insight for the amount of remnant (stick output uncorrelated with the forcing function) that arises from nonlinear pilot technique, and for the remaining remnant arising from different sources unrelated to tracking control (i.e. neuromuscular tremor, re-allocation of cognitive resources, etc.).

1 INTRODUCTION

The earliest study of the human operator as a linear servomechanism is that of Tustin [2] who proposed that, despite amplitude nonlinearities, temporal discontinuities and haphazard fluctuations, there might be an "appropriate linear law" that would describe the main part of the operator's behavior. Insight from servomechanical design led McRuer and Krendel [3] to develop the ubiquitous human Crossover Model (CM), which within its framework accounts for how, and why, the human operator adapts to the controlled plant dynamics during compensatory tracking. With the crossover model, a variable pilot time delay can be used to explain phenomena such as increased high-frequency phase lag associated with increased amounts of error lead equalization. Similarly, ratchet (sustained high frequency, small amplitude pilot-vehicle system oscillations) can be ascribed to variable neuromuscular damping (first proposed by Johnston and McRuer in 1987 [4], and later investigated by Bachelder in 2003 [5] using wavelets). In 1976 Smith [6] propounded that inner-loop rate feedback supported control of the error loop during compensatory tracking, whereby the rate of the controlled system's output was visually perceived by the operator. This manner of feedback was subject to two key constraints: 1) the bandwidth and noise associated with human visual sensing of rate, and 2) the requirement that the ratio of disturbance-to-system output is low, otherwise the error rate that the operator perceives will not correspond to system output rate. A realizable method for perceiving rate for use with inner-loop feedback was first posed by Hess in 1978 [7], whereby the operator employs kinesthetic perception of control rate and an internal model of system response to that rate. This approach was later incorporated into Hess' Structural Model of the human pilot [1,8]. In 1969 Gaines [9] wrote "*Models capable of representing behavior over large domains are particularly important in the study of learning systems where the mode of be-*

havior is expected to vary widely with experience. A variety of models is required, and within the modeling schemata there must be scope for a sufficient variety to provide adequate matches during all phases of learning." Building on Krendel and McRuer's [10] successive organization of perception (SOP) model for tracking skill development, Hess' pilot Structural Model provides a concise, integrated architecture for describing compensatory, pursuit, precognitive, and off-nominal behavior.

The work presented here extends Hess' Structural Model to account for and reproduce pilot compensatory behavior when different control styles are used. It lays the groundwork to explore how pilot control technique (i.e. pulsive versus continuous) influences the interplay between internal costing and the nominal values of a parameter set that defines pilot behavior.

2. STRUCTURAL MODEL OF THE HUMAN PILOT

In 1978 Hess [7] proposed a model (see Fig. 1) for human compensatory tracking whose essential features included an outer loop operating on error (*e*), an inner loop feedback operating on stick position (*δ*), pilot elements that equalize the error and stick signals (respectively Yp_e, $Yp_{\dot{m}}$), a pilot element Yp_n generating the neuromuscular force of the particular limb which drives the manipulator, the manipulator dynamics Y_δ that produces the control system input (usually stick displacement) from the force command, a controlled element Y_c representing the vehicle dynamics, and the display element Y_d that transforms the physical system error to the visually displayed error being tracked. A disturbance *d* is added to the vehicle output *m*, and the negative of this is the error that the operator is attempting to null.

According to McRuer and Krendel [3] the neuromuscular element can be approximated by Eqn (1), where ω_n and ζ_n represent the natural frequency and damping ratio, respectively.

$$Yp_n = \frac{\omega_n 2}{(s^2 + 2\zeta_n\omega_n + \omega_n 2)} \tag{1}$$

With the inner loop of Fig. 1 closed, the simple quadratic form for Yp_n can exhibit the key features of measured high-frequency human controller dynamics, namely, a typically subcritical damping ratio ζn_{CL}, and a minimum second-order amplitude fall-off beyond the undamped natural frequency ωn_{CL}. The injected remnant signal n_e is included to account for nonlinearities and/or time variations in quasilinear fashion.

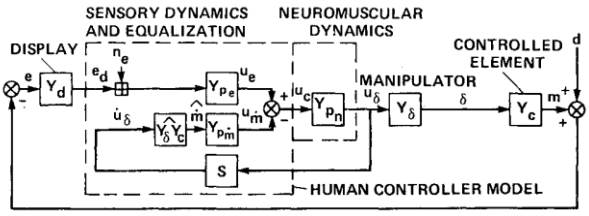

Fig. 1. Quasilinear dual-loop model of the human controller [7].

Typically, the main function of the inner-loop is to provide vehicle output rate feedback and improve stability and precision. Hess proposed (see Fig. 1) that the neuromuscular force output is perceived and transformed into an estimate of vehicle output rate using an internal model of the manipulator and vehicle dynamics suite. For acceleration command dynamics, this process effectively requires the pilot to integrate the force output (in the dual-loop model shown the pilot first perceives the force rate, and integrates this twice). Hess hypothesized that proportional or derivative control in the feedback loop can be conducted using direct information from the muscle spindles and Golgi tendon organs [11], but integral control does not have analogous information and requires the operation to employ higher level cognitive processing [7]. Thus when controlling acceleration command systems, the pilot will tend to generate a pulsive force output rather than a continuous one, since a pulse is the least difficult of all waveforms to integrate (an impulse is even easier, but is a variation of the pulse). While the pulse is held, the system response is the inverse Laplace transform (L^{-1}) of the integral of the vehicle dynamics (for acceleration command system, this would be L^{-1}(K/s^3)). Following the pulse, the system response is simply the inverse Laplace transform of the vehicle dynamics, L^{-1}(K/s^2). "Ease of integrability" can be generally interpreted in a physiological sense as applying to those waveforms whose integration requires a minimum of higher-level activity in the central nervous system [12].

As an operator becomes familiar (gains expertise) with the vehicle and manipulator, the transformation between force output and vehicle output rate should reduce to a one-step process. In his

revised Structural Model [1], Hess reflects this simplification with a proprioceptive feedback element, Y_{PF}, shown in Fig. 2. This element receives stick position (δ_M), and depending on the vehicle dynamics in the vicinity of the crossover frequency, Y_{PF} will assume one of the forms shown in Table 1 (to approximately generate $\dot{M}$, the rate of the output). The vehicle dynamics in Table 1 are position, rate, and acceleration command, respectively, and the corresponding Y_{PF} is a first-order lead, proportional, and first-order lag, respectively.

Table 1. Proprioceptive feedback element Y_{PF} form.

Vehicle Dynamics	K_v	K_v/s	K_v/s^2
Y_{PF}	$K_\delta(s+a)$	K_δ	$K_\delta/(s+a)$

In manual control theory, *proprioception* refers to the monitoring of body's actions– excluding the visual and vestibular systems. The kinesthetic system is a subsystem of the proprioceptive system, dedicated to the perception of position and movement. In this paper proprioceptive and kinesthetic input will be used interchangeably. A gain K_e serves as the pilot element acting on error, and the neuromuscular and feel system elements are respectively denoted by Y_{NM} and Y_{FS}. Note that Y_{NM} in Fig. 2 is Yp_n in Fig. 1. While the various other details of the Structural Model (Fig. 2) are described in [1], an element of key importance is the central processing time delay τ_o, which for a given pilot is approximated as vehicle-invariant. This represents a major simplification to the crossover model's effective time delay, which was used to explain (but could not predict) task and vehicle-dependent high frequency phase loss.

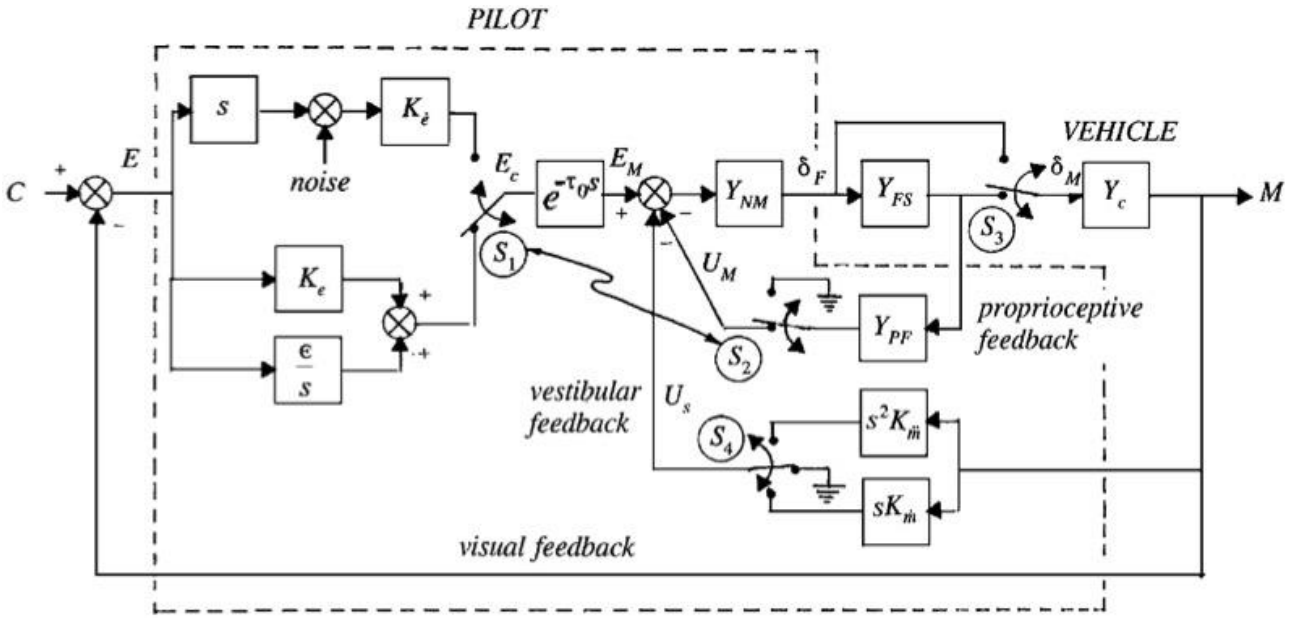

Fig. 2. Structural Model of the Human Pilot [13].

Fig. 3 reduces the Structural Model to the components relevant for fixed-base compensatory control (hence the vestibular paths are removed), with two modifications. The pilot element operating on the error channel is now represented by Y_e, and a pilot element Y_{TECH} has been added just prior to Y_{NM}. Hess employed a similar element in his Dual Loop model [12] to account for pulsive response. In Fig. 3, Y_e appears as a first-order lead instead of the pure gain of Fig. 2. - this form allows more adaptive error equalization, and it is seen in earlier versions of the Structural Model. Y_{TECH} represents the logic generating a pilot's non-linear control technique, which can be a set of conditionals and the supporting computations. The vehicle dynamics used in the following example cases will either be acceleration or jerk command dynamics, consequently Y_{PF} for both will be a first-order lag (see Table 1).

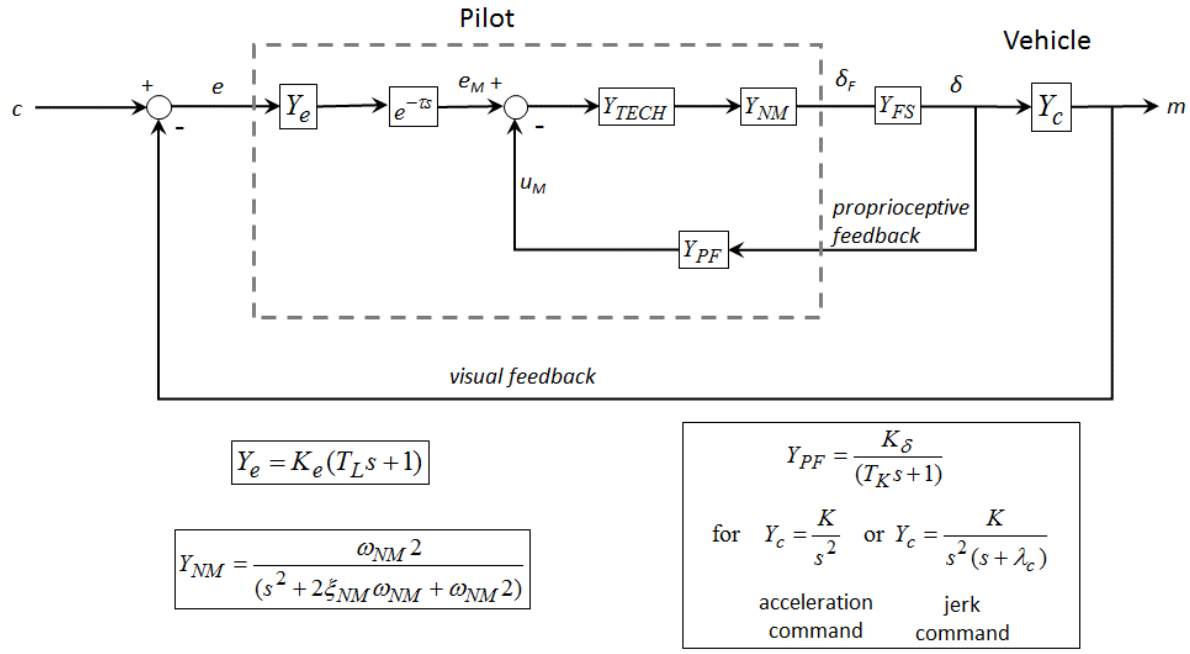

Fig. 3. Pilot Structural Model simplified for fixed-base tracking.

3 WORKLOAD EXPERIMENT

An experiment was conducted that investigated the relationship between aircraft input/output states and pilot workload. Four command vehicle dynamics (proportional, rate, acceleration, jerk), vehicle gains (vehicle sensitivity to input), and display gains (display sensitivity to error) were used with a lateral station-keeping using a compensatory display, where a random forcing function continuously disturbed ownship's position.

Fig. 4a shows a representation of the station-keeping task and the display (K_D), pilot (Y_P) and vehicle (Y_V) components of the closed-loop system. Fig. 4b gives the range of conditions within each component that were tested. The jerk condition for the vehicle dynamics (fourth condition listed for Y_V), contains a pole p whose location was varied. Twenty-three display configurations were tested with each subject using various combinations of the conditions shown in Fig. 4b. The configurations were selected to maximally span the Bedford rating over all vehicle command dynamics. Since pilot proficiency with any test condition was not a factor in this experiment, pilots were given two practice of each vehicle dynamic type (proportional, rate, acceleration, jerk) prior to testing.

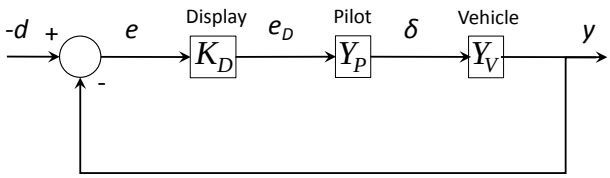

a.

$$Y_V = \left\{ K_V,\ \frac{K_V}{s},\ \frac{K_V}{s^2},\ \frac{K_V}{(s+p)s^2} \right\}$$

$$K_V = \{5, 10, 30, 60\} \quad p = \{1, 2, 5\}$$

$$K_D = \{0.5, 2, 4, 8, 32\}$$

b.

Fig. 4. Station-keeping task. a) Pilot, display, and vehicle elements; b) Range of conditions for display and vehicle elements.

One may be tempted to think that the display gain and the vehicle gain are effectively interchangeable and the same gains from the pilot's vantage point. The following example will serve to disprove this common misnomer. If the pilot's input is zero, the disturbance is perceived through the display gain – the vehicle gain does not come into play at all. Based on his/her control activity and quiescence, a pilot learns to decouple the effects of the display gain from the vehicle gain – thus decoupling aircraft motion due to disturbance from pilot-commanded vehicle motion.

Four male participants took part in the study. Three were Experimental Test Pilots (graduates of Navy Test Pilot School) with 1,900, 1,900, and 2,450 rotary wing flight hours. The fourth participant had logged 800 hours of rotary wing flight time. Ownship error relative to the target location was displayed on a laptop monitor (see Fig. 5), and the pilot attempted to minimize the error using a gamepad joystick (Logitech Dual Action gamepad). The Bedford rating scale [14] was used to subjectively score each pilots spare capacity at the end of each 60-second tracking run. Dependent qualitative variables were: stick position, rate and acceleration, stick position reversals, display error, rate, and acceleration. The positional disturbances imposed on the helicopter were designed to be both realistic and a diagnostic probe for pilot control behavior. Composed of a sum of 11 non-harmonically-related sine waves, the disturbance was perceived by the pilot as a random process – the result, however, was that the pilot's control response power resided largely at the same frequencies contained in the input disturbances. Sum-of-sines (SOS) is a standard approach that has been employed by the manual control research community over many decades. The disturbance time history is shown in Fig. 5 (it ranged from approximately -1 to 3 feet, with a standard deviation of 1 foot). The results of the experiment are given in [15].

The damped frequency of the gamepad joystick was approximately 200 rad/sec, well above the neuromuscular mode. Thus the feel system Y_{FS} in Fig. 3 can be considered unity for this experiment.

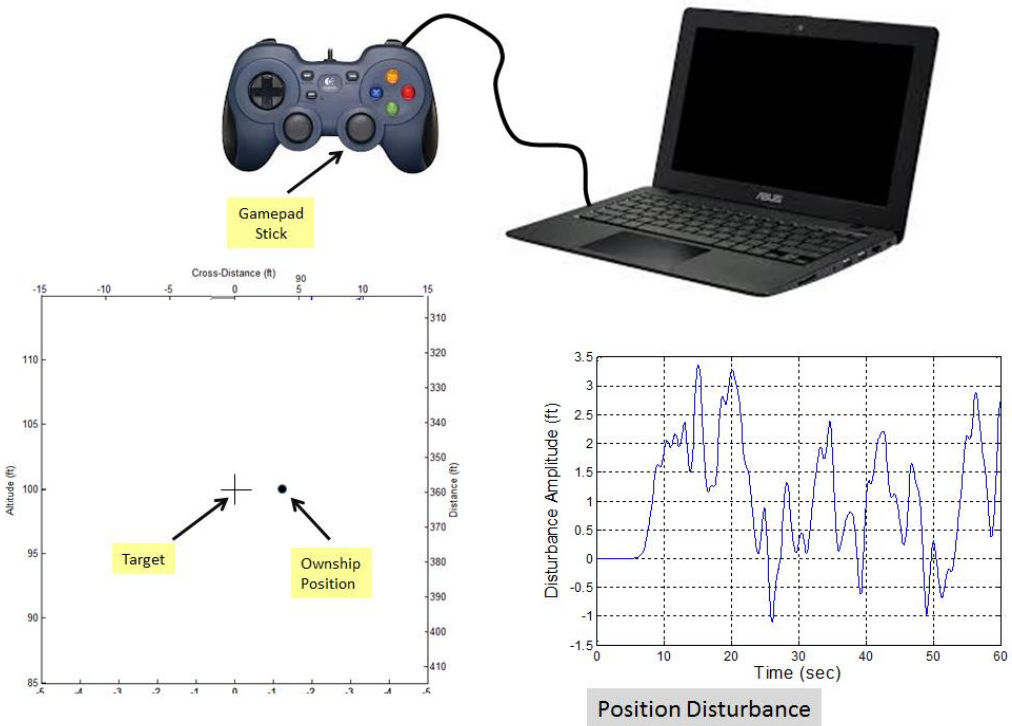

Fig. 5. Simulation environment.

4 PULSIVE MODEL DEVELOPMENT

In the experiment two pilots were observed to use different pulse techniques when controlling the acceleration and jerk command dynamics. Fig. 6a shows the pulse width modulation (PWM) technique, where the gamepad joystick was rapidly deflected to the stops and released, so that pulse firing and pulse width were predominantly the only two control variables. In digital control PWM creates a square wave, a signal switched between on and off, to create analog results with digital means. Fig. 6b shows the pulse width-amplitude modulation (PWAM) technique (coined by the author), where stick motion consists of pulses for motion that reaches the stops, and amplitude-varying impulses otherwise.

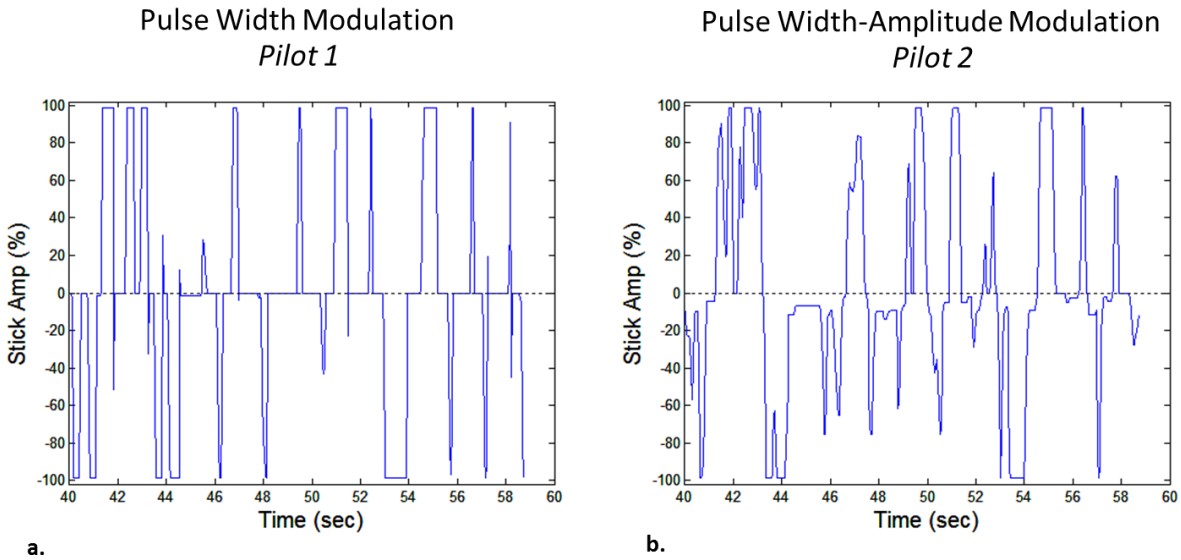

Fig. 6. Pilot control techniques used in tracking task. a) Pulse width modulation; b) Pulse width-amplitude modulation.

At the time that the pulse models were developed the CM was used to characterize the pilot element. Both the Structural Model and the CM yield equivalent frequency responses for the pilot (δ/e in Fig. 7a) in the region of crossover frequency ω_c [7]. The following describes the procedure that was employed to recognize and formulate the pulse logic for both the PWM and PWAM techniques. The open loop frequency response (y/e in Fig. 7a) was computed, from which the ω_c and the effective time delay τ were estimated. Assuming the pilot acts like a first-order lead with a time delay (see Y_p in Fig. 7a), when crossover occurs K can be written in terms of known constants and the unknown lead term T_L. This is substituted back into Y_p so that the only unknown is T_L, and a best-fit is performed (solid blue line in Fig. 7b) with pilot's magnitude and phase (filled circles in Fig. 7b) to yield T_L, hence Y_p. The output of Y_p is termed the CM stick response, and this was computed in time over the run and compared with the actual stick pulses (Fig. 7c). It was observed that in general a pulse is triggered by zero-crossings and opening speed reversals (i.e. away from zero) in the CM stick response. Fig. 7c also shows a pulse that does not correlate with either a zero crossing or an opening speed reversal, and this kind of pulse occurred often enough to warrant examining its trigger source.

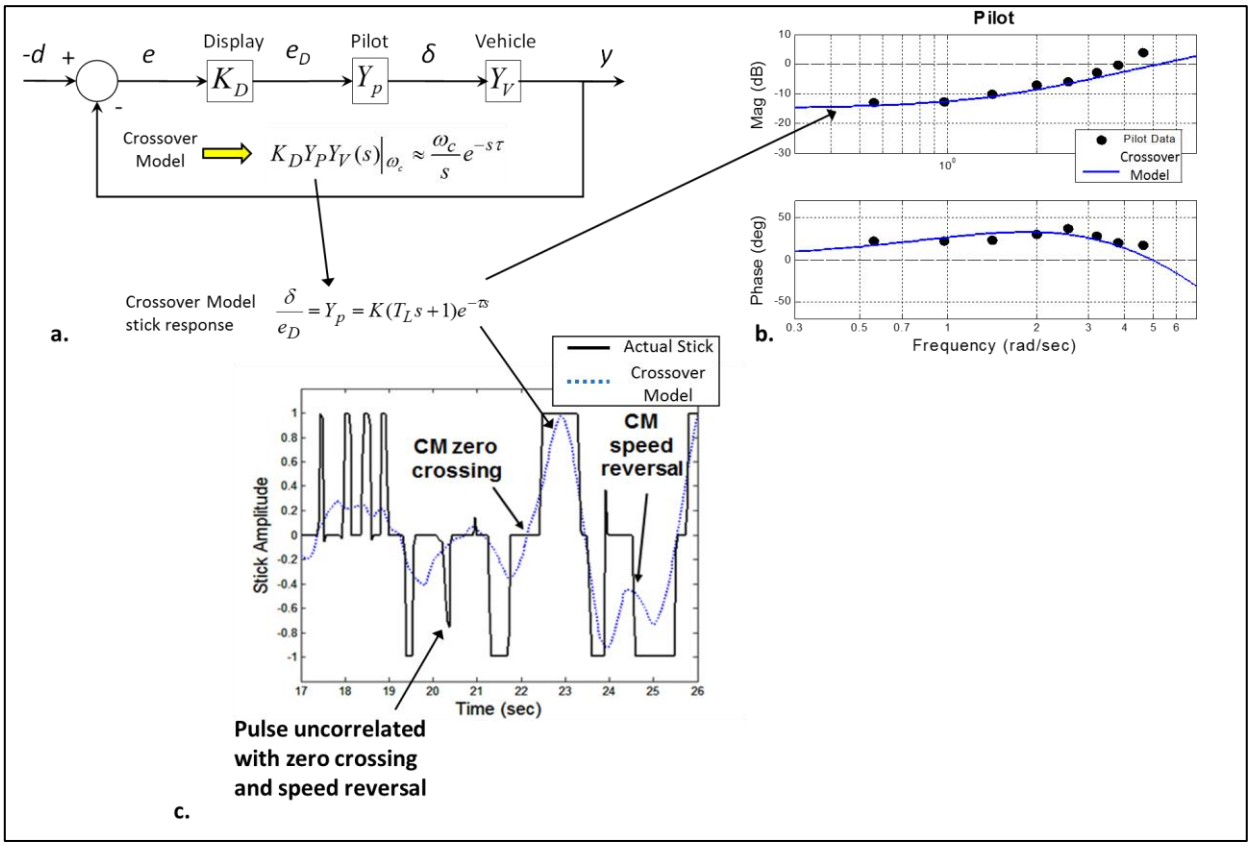

Fig. 7. CM employment for PWM logic identification. a) Basic CM elements; b) Identified pilot frequency response for PWM technique; c) CM stick signal overlaid on actual stick history showing correspondence between pulsing and CM's stick signal.

In Fig. 8b the areas under actual and crossover stick signals are integrated in time, with integration starting and ending when the sticks change polarity. It is seen that the integrations approximately match when the stick polarities flip. By inspection pulses were observed to obey the logic shown at top of Fig. 8, where a pulse ceases if the area under the actual stick is greater than some fixed percentage of the area under the crossover model's signal. Pulses are triggered when the crossover model's stick encounters a zero crossing or opening speed reversal, or when the area under the actual stick is less than some fixed percentage of the area under the crossover model's signal. It was also observed that there is generally consistent a delay between when a zero crossing or opening speed reversal occurs, and when a pulse is actually triggered. This appears to be a safeguard against spurious triggering by requiring a certain amount of time to pass and for the amplitude to rise above some minimum threshold before the operator commits to a pulse.

The logic governing PWAM was similar to PWM, except that the variable pulse amplitude was assigned to be the CM's stick amplitude at the time of pulse trigger, multiplied by a constant. Fig. 9 compares the modeled and actual stick outputs for the PWM and PWAM styles, and they subjectively appear to agree well. In the next section, modeled and actual behavior will be compared using frequency response, as well as probability distributions of the stick amplitude and periods of stick inactivity (quiescence).

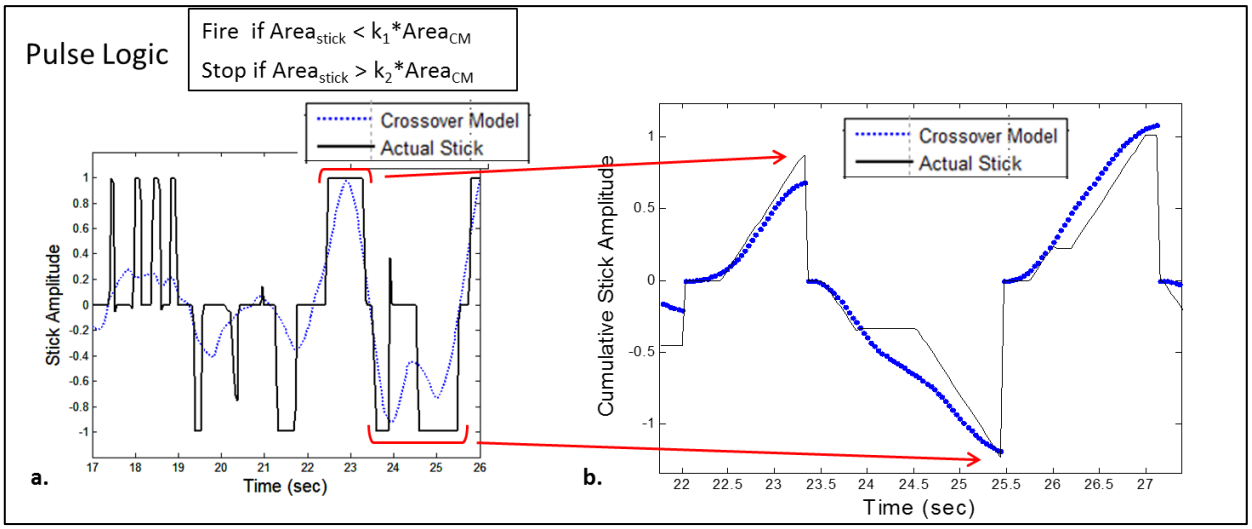

Fig. 8. PWM Crossover Model and stick integration. a) CM stick signal overlaid on actual stick; b) Comparison CM integration and actual stick integration (they are roughly equal at each zero crossing of the CM output). Pulse logic shown at top, governing pulse width and pulses not associated with zero crossing and opening speed reversal.

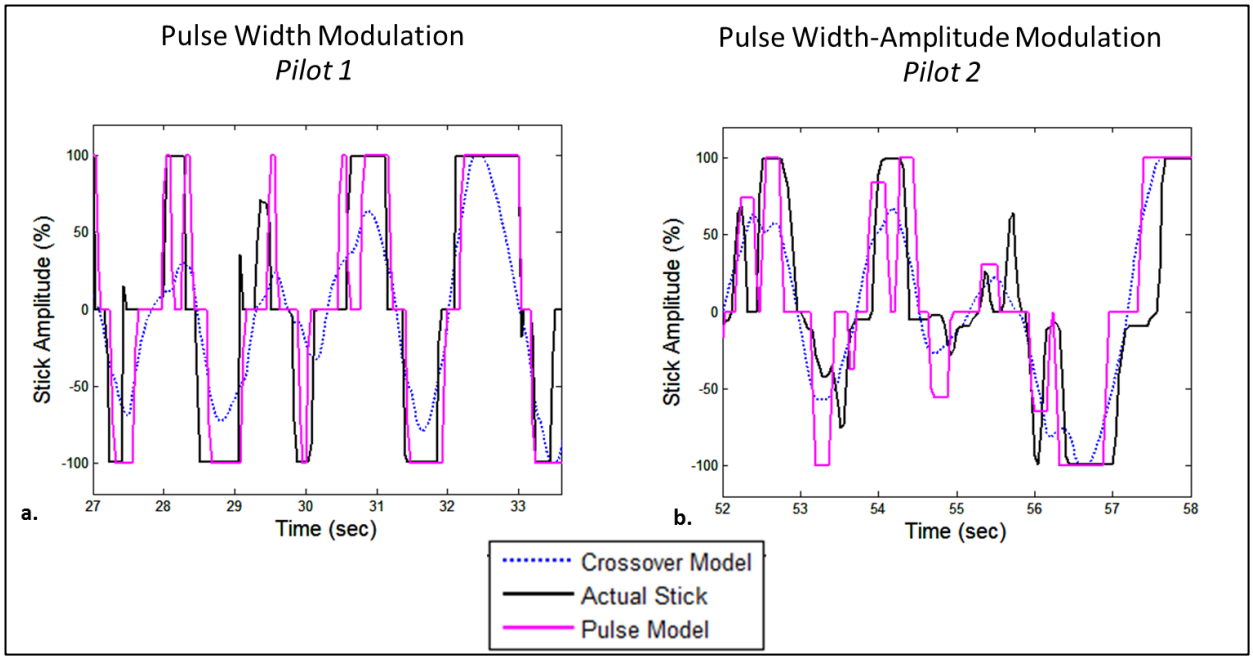

Fig. 9. Comparison of pulse models with actual data: a) Pulse Width Modulation; b) Pulse Width Amplitude Modulation.

5 MODEL VERIFICATION

Bachelder and Aponso [15] identified a nonlinear pilot control technique termed 'amplitude clipping,' whereby the pilot responds to error as predicted by the CM up to a certain stick amplitude and then holds that amplitude until the error signal reverses and returns, at which time the pilot resumes active continuous tracking. The amplitude at which the control input is capped can vary over time. Examples are now given where Structural Model was used to identify the pilot element for the PWM, PWAM, and amplitude clipping control techniques.

Rather than iterate on the undamped natural frequency of the open loop neuromuscular system (ω_{NM}) along with the other parameters of the

Structural Model (Fig. 3) until a best-fit with the observed data is obtained (or fixing ω_{NM} at some assumed value), the power spectrum of pilot's stick was examined. Fig. 10a shows the power spectrum density (PSD) of the stick when amplitude clipping was used to control acceleration command dynamics. The frequencies of the SOS forcing function are denoted with open circles, the highest frequency located approximately at 5 rad/sec. Fig. 10b is a close-up beyond 5 rad/sec, and power can be observed up to about 10 rad/sec, showing a concentration at around 7 rad/sec. When jerk-command dynamics are controlled (again using amplitude clipping), Fig. 10d shows the power to be more evenly distributed between 5 and 10 rad/sec. Based on these observations, ω_{NM} was fixed at 8 rad/sec when amplitude clipping was used as the control style. This is lower than the value used by Hess in [8], which is likely due to the different inceptor and limb characteristics (the gamepad joystick is controlled by the thumb).

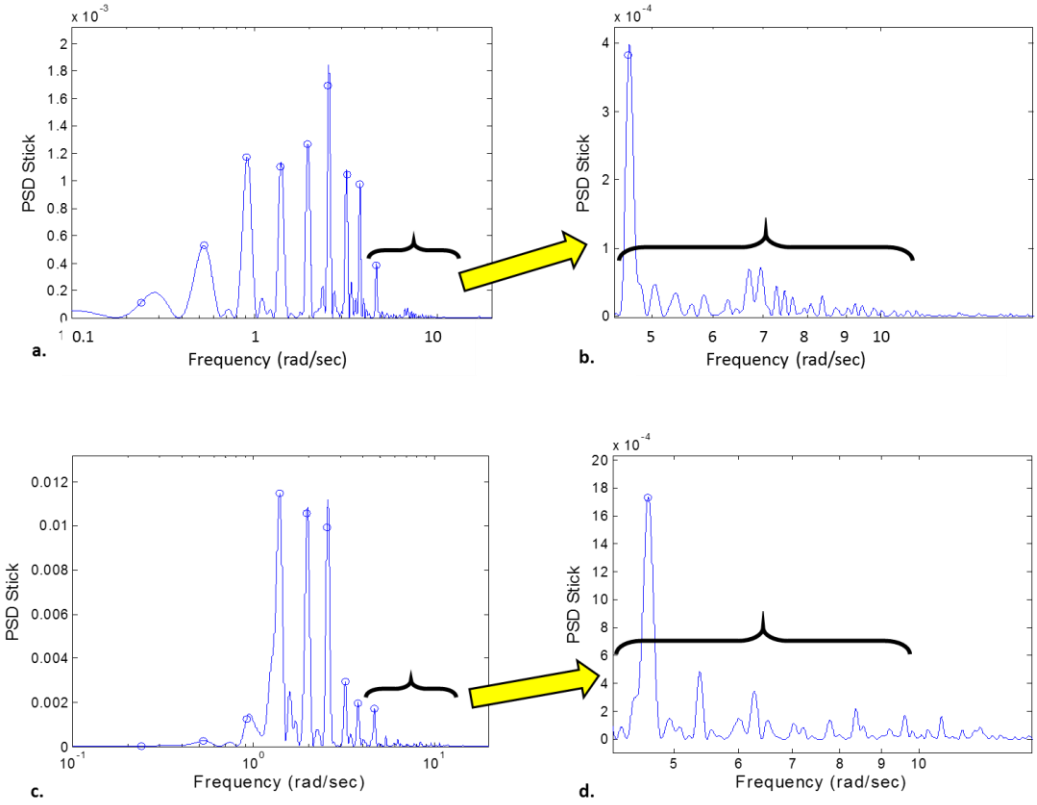

Fig. 10. Spectral decomposition of stick response: a) Using acceleration-command vehicle dynamics (forcing function power denoted by open circles); b) Close-up beyond the forcing function power. c) Using jerk-command vehicle dynamics; b) Close-up beyond the forcing function power.

Using the delay employed in [8], the pilot time delay was fixed at 0.20 seconds, and the five other parameters of the pilot Structural Model (K_e, T_L, K_δ, T_K, ς_{NM}) were iterated in a Simulink model of Fig. 3 to minimize the cost function J given in Eqn. 2.

(2) $$J = [\gamma_1 * \sum_{i=1}^{8} \Delta mag_i^{YpYv} + \gamma_2 * \sum_{i=1}^{8} \Delta phs_i^{YpYv} + \gamma_1 * \sum_{i=1}^{8} \Delta mag_i^{Yp} + \gamma_2 * \sum_{i=1}^{8} \Delta phs_i^{Yp} + \gamma_3 * \Delta\sigma(\delta) + \gamma_4 * \Delta PDF]$$

In Eqn 2, Δ( ) refers to the absolute difference between observed and simulated variable ( ). Δmag_i^{YpYv} thus denotes the difference in the

open loop magnitudes ($YpYv$, in dB) between observed and simulated at each frequency i of the forcing function, Δphs_i^{YpYv} denotes the difference in the open loop phase, and Δmag_i^{Yp} and Δphs_i^{Yp} use the magnitude and phase of the pilot element, respectively. $\sigma(\delta)$ is the standard deviation of the stick, and *PDF* is the probability density function of the stick amplitude (see Fig. 13a). The elements in Eqn 2 are weighted by constants γ. The time domain metrics (σ and *PDF*) were included since it is possible for a very different stick power distribution and σ to produce the same frequency response.

Four runs from the workload experiment are used to examine the pilot models. Three runs use the same display, stick, and vehicle dynamics (vehicle is acceleration-command), and are flown by three different pilots: one employing the PWM technique, the second PWAM, and the third amplitude clipping (AC). The fourth run used AC and jerk-command dynamics, flown by the same pilot who employed AC with acceleration-command dynamics. These four runs were selected to highlight differences due to techniques and vehicle dynamics. The parameters minimizing the cost function for four simulation runs are given in Table 2, along with various metrics. The estimated Bedford rating (computed from the modeled response as described in [15]), B_{est}, and the actual Bedford rating are given in Table 2. Also compared is the relative correlated output ρ^2, defined as the portion of the power in the stick output which exists at the disturbance frequencies, divided by the total stick power. For instance, in Fig. 10a, summing the areas flanking each forcing frequency (out to the first local minimum in PSD) yields the correlated power, and this is divided by the total PSD area.

Fig. 11 shows the identified open loop and pilot frequency responses (computed using cross spectral densities, [3]) from the observed pilot data and from the data generated by the nonlinear simulation (nonlinear due to the pilot technique element Y_{TECH}). This example employed acceleration-command dynamics, and the pilot technique was amplitude clipping. The solid line denotes the linear frequency response produced without the nonlinear pilot technique element. The nonlinear effects of clipping are minimal except at the lower frequencies, where magnitude is reduced.

Looking at Table 2 the relative correlated output ρ^2 for the simulation is 0.93, also reflecting the technique's minimal impact on remnant. Note that the actual value of ρ^2 was 0.85, suggesting that the pilot's contribution to remnant due to internally generated noise is approximately 8% (0.93-0.85) of the total stick power. Without an accurate model of pilot technique, the 15% total remnant observed from the pilot data could not have been partitioned into technique and internal noise.

Table 2. Pilot model parameter values used to generate describing functions, and comparison of simulated and actual measures.

Controlled-element dynamics	Control technique	K_e	T_L	K_δ	T_K	τ	ζ_n	ω_n	$\sigma(\delta_{sim})$	$\sigma(\delta_{act})$	$\sigma(e_{sim})$	$\sigma(e_{act})$	ρ^2_{sim}	ρ^2_{act}	B_{est}	B_{act}
K/s^2	AC	0.19	0.96	0	-	0.20	0.3	8	0.32	0.33	1.00	1.10	0.93	0.85	6.4	6
K/s^2	PWAM	0.40	0.60	0.25	0.43	0.20	0.3	8	0.43	0.43	0.86	0.95	0.76	0.72	6.2	6
K/s^2	PWM	0.25	0.80	0.10	0.48	0.20	0.3	8	0.60	0.60	0.87	1.10	0.67	0.67	6.8	6
$K/s^2(s+3)$	AC	0.35	0.55	0.10	1.13	0.20	0.3	8	0.43	0.47	1.36	1.84	0.94	0.83	8.5	8

K_e: Pilot (Yp_e) gain, error channel
T_L: Pilot (Yp_e) lead time constant, error channel
K_δ: Pilot (Yp_δ) gain, stick channel
T_K: Pilot (Yp_δ) lead, time constant, stick channel
ζ_n: Neuromuscular damping
ω_n: Neuromuscular frequency (rad/s)
σ: Standard deviation
ρ^2: Relative correlated output
B: Bedford rating

Fig. 12 shows good correspondence between the time histories of the actual and simulated stick amplitudes. Actual and simulated stick PDFs compare favorably in Fig. 13a, as does the distribution of quiescence time in Fig. 13b. Quiescence was defined as when the stick's rate fell below a threshold, when stick amplitudes were non-zero (i.e. time did not accrue towards quiescence when the stick was in the zero-force, zero-amplitude position). The metrics for this run in Table 2 (K/s^2 dynamics, AC denotes amplitude clipping), in combination with Fig. 11 - Fig. 13, indicate that the integrated components of the model reproduced the pilot's response with high accuracy. Of note is that the pilot did not employ the kinesthetic feedback loop (K_δ was zero), instead equalizing the error channel with only gain and lead.

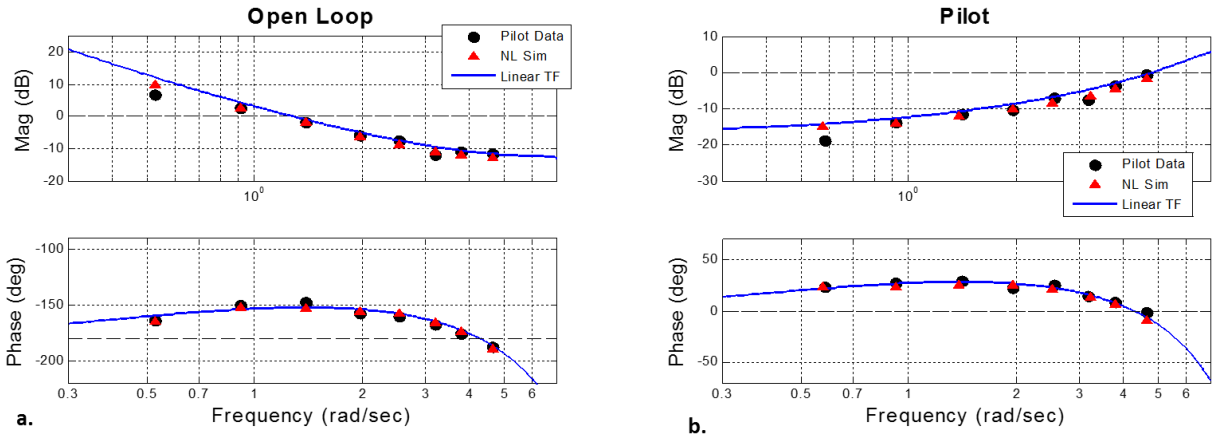

Fig. 11. Identified open loop and pilot frequency responses for the pilot data and nonlinear model data, with the linear model overlaid (acceleration-command dynamics, Amplitude-Clipping model). Note the difference in scale between Open Loop and Pilot responses.

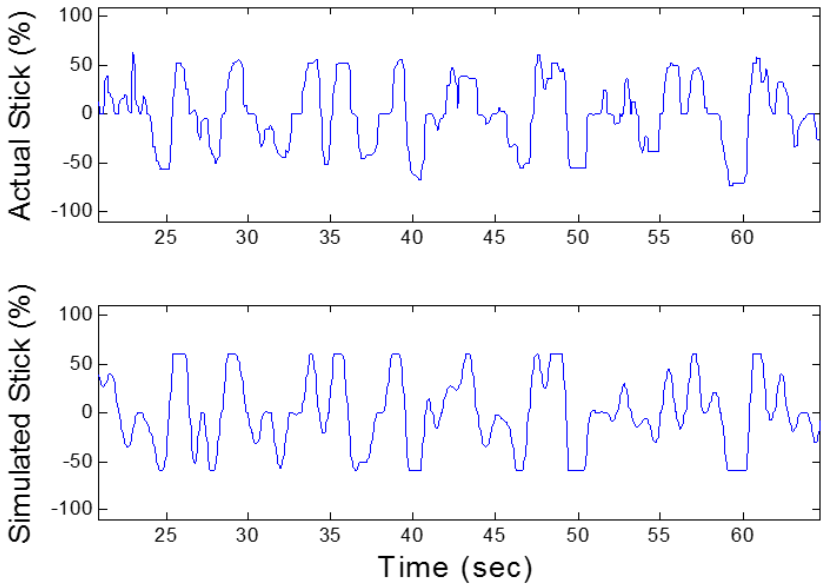

Fig. 12. Comparison of actual and simulated stick (acceleration-command dynamics, Amplitude-Clipping model).

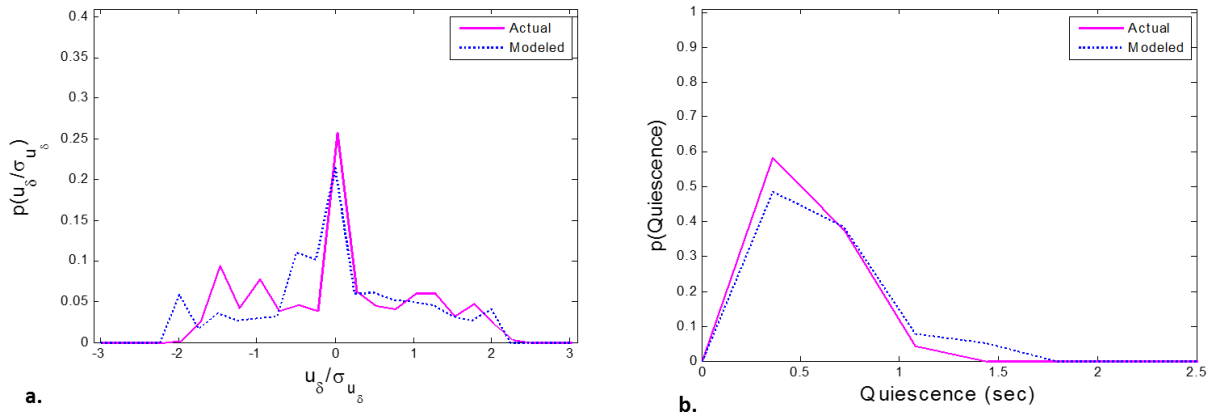

Fig. 13. Distributions for stick associated with Fig. 12 comparing actual and model: a) Stick amplitude distribution; b) Stick quiescence distribution.

Simulation of the control style PWAM in the Structural Model is now examined. The sharp edges and corners observed in the stick response for both PWM and PWAM control infer that their neuromuscular dynamics affected frequencies far higher than what was measured when amplitude clipping (pseudo-continuous) control is used. When the joystick stops are reached (+/- 100%) the neuromuscular mode does not factor at all. The neuromuscular pilot element Y_{NM} was thus set to unity when modeling PWM and PWAM, eliminating ω_{NM} and ζ_{NM} from the identification process. Fig. 14 shows good model agreement with the actual frequency and time responses. The linear response (i.e. when the pilot technique element is left out) in Fig. 14b illustrates how high-fidelity modeling can expose observed measurements as artifacts of technique rather than the result of internal processing. McRuer [3] describes the phenomenon of low frequency 'droop' observed in pilots, which was not accounted for by the basic CM. This low frequency phase loss increased with the order of the system being controlled, and in [7] was attributed to and reproduced using the inner kinesthetic feedback loop. However, in this run the marked difference in phase (and magnitude) between the linear response and the nonlinear response at the lowest frequency is due entirely due to the PWAM technique. If the kinesthetic feedback were contributing to the phase and magnitude droop this would have caused the linear response to move toward the modeled nonlinear response. The actual measured phase agrees with the nonlinear model, including at the higher frequencies where the pilot phase also departs from the linear response. Phase droop also occurs with rate and position command dynamics [3], where continuous control would certainly be employed and technique would not be a factor, but this example highlights the potential importance of including pilot technique when assigning causality.

Looking at Table 2, the pilot made substantial use of inner-loop proprioceptive feedback (K_δ = 0.25), and remnant due to technique (1- ρ^2_{sim} = 24%) was considerably larger than when amplitude clipping was employed by the other pilot (where 1- ρ^2_{sim} = 7%). Despite the seemingly stochastic nature of PWAM, the pilot's internal remnant (4%) was half the internal noise associated with the amplitude clipping technique. This is quite remarkable given that the pilot appears to be *simultaneously* integrating both the physical stick position as well as the internally-generated stick position to generate the pulse commands (see Fig. 8).

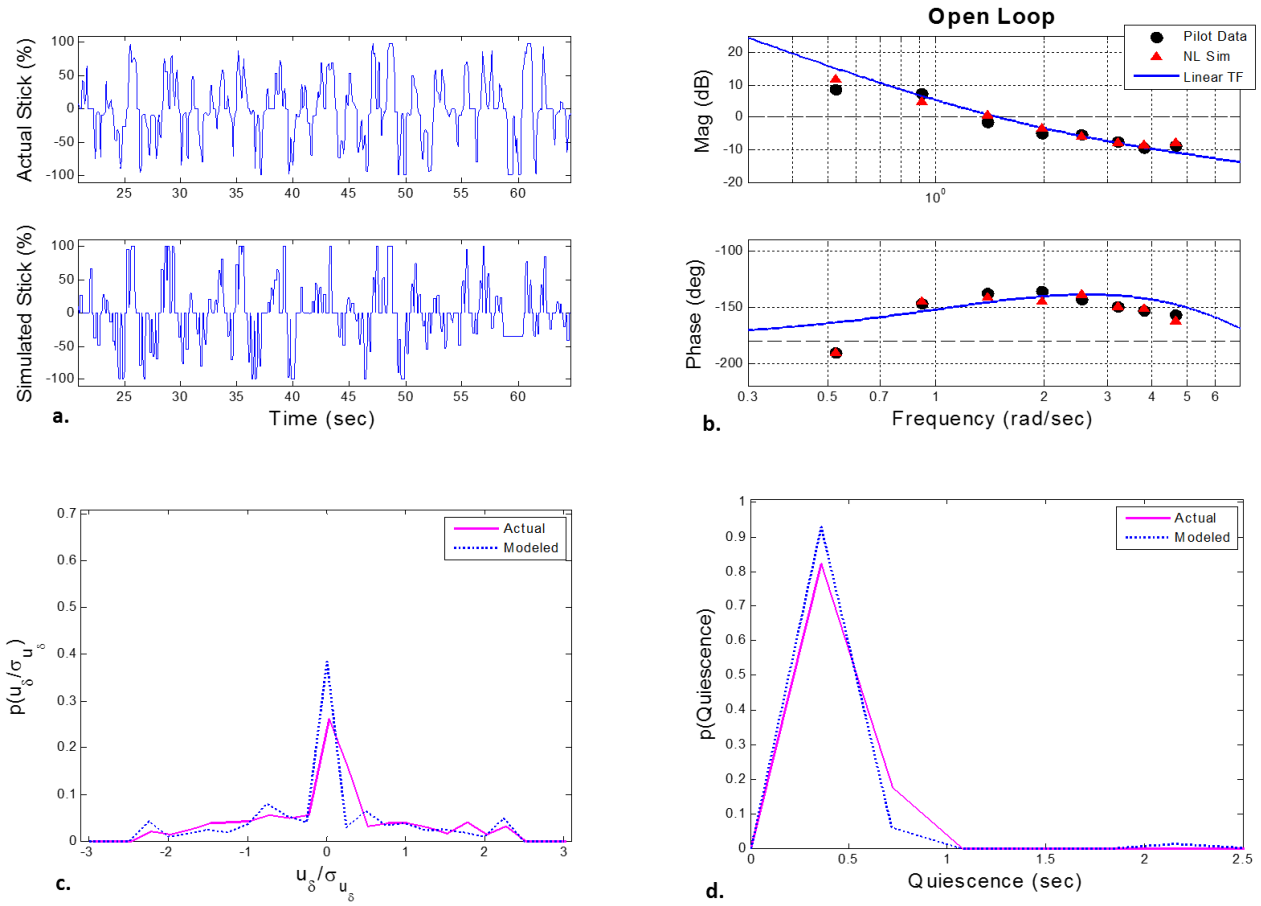

Fig. 14. Pulse Width Amplitude Modulation (acceleration command dynamics): a) Comparison of actual and simulated stick; b) Frequency response comparison of open-loop; c) Stick amplitude distribution; d) Stick quiescence distribution.

The frequency and time domain results in Fig. 15 show excellent correspondence between modeled and pilot data for PWM control. The simulated PWM control technique produced 33% remnant, and since this coincided with the remnant observed in the experimental data then the pilot apparently generated almost no internal noise (given the model's accuracy). The technique also appears to be responsible for the leveling of magnitude at the higher frequencies (note the observed and nonlinear model magnitudes match, departing from the linear response in Fig. 15). Kinesthetic feedback was activated (K_δ =0.10), but to a lesser extent than with PWAM.

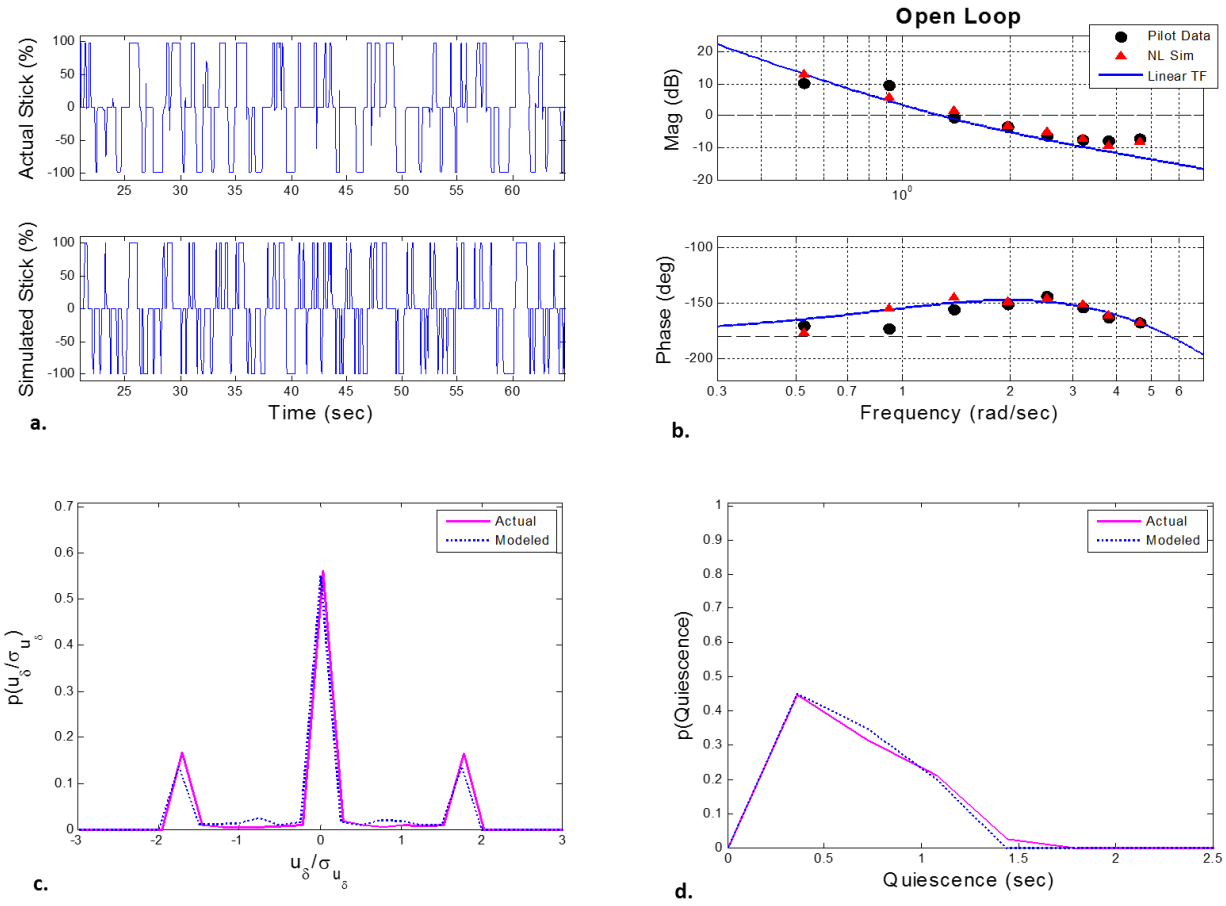

Fig. 15. Pulse Width Modulation (acceleration command dynamics): a) Comparison of actual and simulated stick; b) Frequency response comparison of open-loop; c) Stick amplitude distribution; d) Stick quiescence distribution.

The last example examines a run that employed amplitude clipping to control jerk dynamics - dynamics which are extremely challenging to stabilize and to conduct tracking with. In Fig. 16 the model produced a good match with the pilot data in frequency response and stick amplitude distribution, and a fair match in the time response and quiescence distribution. The internal noise (ρ^2_{sim} - ρ^2_{act}) of the pilot is the highest (11%) out of the four runs presented, and in contrast to when this pilot was controlling acceleration command dynamics, he now employed proprioceptive feedback (K_δ = 0.10) and generated the largest lag time constant (T_K=1.13, more than double what the other two pilots operated at).

With the evidence suggesting that both PWM and PWAM integrate the internal stick signal and the physical stick position (Fig. 8b), the Structural Model has been modified (Fig. 17) with technique-dependent switches that can enable the integration paths to the pilot technique element when needed. Since the two pulsive techniques required pure kinesthetic integration of the stick, it seems reasonable to assume that this same information would be employed by the first-order lag in the kinesthetic feedback loop (see Y_{PF} in Fig. 3). Coincidentally PWM and PWAM were both observed to employ this loop.

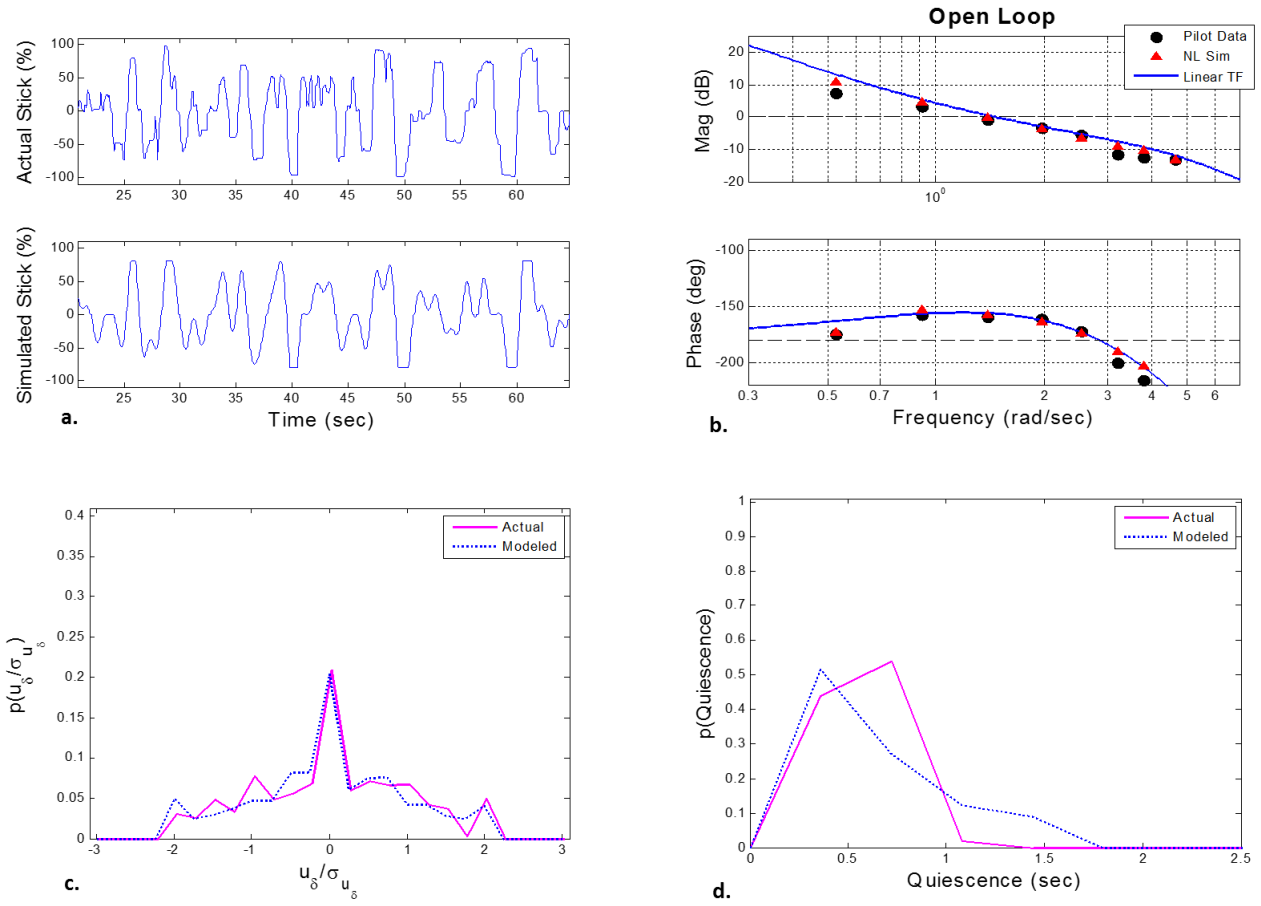

Fig. 16. Amplitude Clipping (jerk command dynamics): a) Comparison of actual and simulated stick; b) Frequency response comparison of open-loop; c) Stick amplitude distribution; d) Stick quiescence distribution.

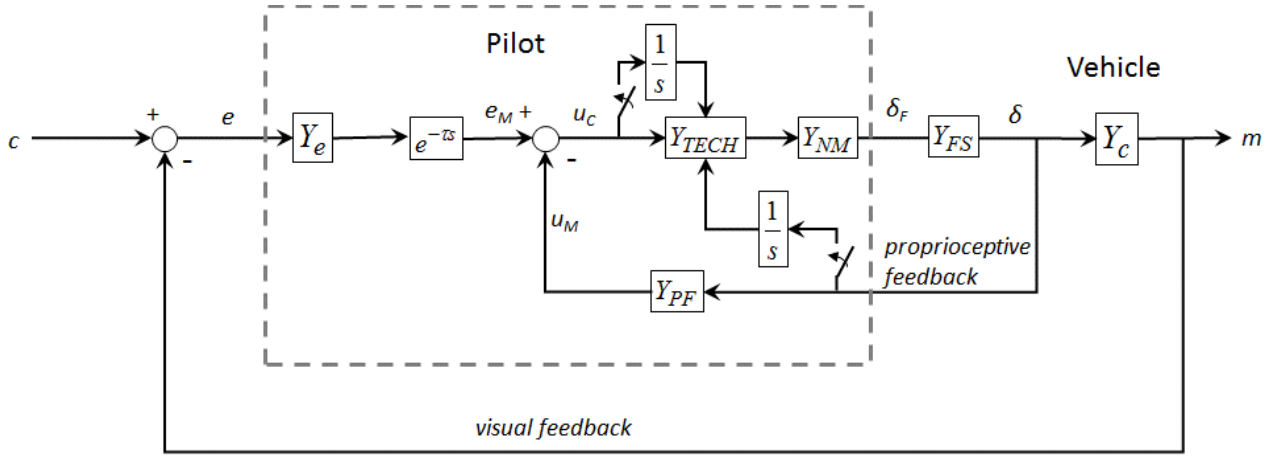

Fig. 17. Pilot Structural Model showing integration of internal stick and physical stick signals as technique-dependent inputs to the pilot technique element.

6 CONCLUSIONS

Two models representing two types of observed pilot pulsive behavior – pulse width modulation (PWM), and pulse width amplitude modulation (PWAM) – were developed. These two pulsive models and a third nonlinear model (amplitude-clipped continuous control) were analyzed using pilot data Hess' pilot Structural Model. Preliminary results suggest:

1) The pulsive models used in conjunction with the pilot Structural Model closely reproduced the pilot data both in the frequency and time domains during closed-loop simulation. This suggests that for the range of tasks and control styles encountered, the models captured the fundamental mechanisms governing pulsive and control processes.
2) Pulsing can produce artifacts such as low frequency droop that may appear as characteristics internal to the pilot when they are the result of control technique. Accurate modeling can identify such artifacts.
3) The pulse models developed give important insight for the amount of remnant (stick output uncorrelated with the forcing function) that arises from nonlinear pilot technique, and for the remaining remnant arising from different sources unrelated to tracking control (i.e. neuromuscular tremor, etc.).
4) In addition to emulating observed pilot behavior, the pilot Structural Model provides a method of economy for modeling higher frequency response. By assuming an invariant pilot time delay and neuromuscular damping, and using the stick power spectrum to estimate the neuromuscular natural frequency, kinesthetic feedback systematically emulated high frequency phase loss. In contrast, the single-loop CM accounts for this phase loss using an effective time delay, which is roughly attributed to increased level of difficulty.
5) During pulsive control of K/s^2 (acceleration command) vehicle dynamics, it appears that skilled pilots: 1) produce a continuous, internally-generated stick signal that they integrated in time; 2) integrate the actual stick position; and 3) compare the two integrations to issue or cease a pulse command. Since the two pulsive techniques (PWM and PWAM) required pure kinesthetic integration of the stick, it seems reasonable to assume that this same information could be employed by the first-order lag in the kinesthetic feedback loop. Both pulsive techniques were observed to use this loop.
6) The pilot employing PWM rapidly deflected the gamepad's joystick to the stops (i.e. maximum deflection), producing sharply-edged and cornered pulses. The PWAM style employed both this technique and a train of spikes, where the stick impulsively rose to some peak amplitude and rapidly return to zero when released. The best matching between the modeled and observed behavior (PWM and PWAM) was obtained by setting the neuromuscular pilot element Y_{NM} to unity, implying that those techniques were largely unaffected by the neuromuscular constraints typically associated with manual tracking. Thus pulsing can present a method for ameliorating unfavorable stick characteristics.

The cases explored in this study are too few to offer statistically significant results, rather they are intended to provide insight and guidance for future research.

Acknowledgments

This work was supported by cooperative agreement NNX16AJ91A between the U.S. Army Aviation Development Directorate and San Jose State University. This paper has been approved for public release: unlimited distribution.

REFERENCES

1 Hess, R. A., "Unified Theory for Aircraft Handling Qualities and Adverse Aircraft-Pilot Coupling", Journal of Guidance, Control, and Dynamics, Vol. 20, No. 6, 1997.

2 Tustin, A., “The nature of the human operators response in manual control and its implication for controller design,” J. Instn. Elect. Engrs, 94, 190, 1947.

3 McRuer, D. T. and Krendel, E. S., “Mathematical Models of Human Pilot Behavior," No. AGARDograph No. 188, November 1973.

4 Johnston, D.E., and McRuer, D. T., "Investigation of Limb-Side Stick Dynamic Interaction with Roll Control," Journal of Guidance, Control, and Dynamics, Vol 10, No 2, March-April 1987, pp 178-186.

5 Bachelder, E. N., and Klyde, D. H., “Wavelet-Based Analysis of Roll Ratchet Using a Flight Test Database,” AIAA 2003-5692 presented at AIAA Atmospheric Flight Mechanics Conference, Austin, TX, August 11-14, 2003.

6 Smith, R. H., "A Unified Theory for Pilot Opinion Rating, "Proceedings of the Twelfth Annual Conference on Manual Control, May 1976, pp. 542-558.

7 R. A. Hess, "A Dual-Loop Model of the Human Controller," Journal of Guidance, Control, and Dynamics, vol. 1, pp. 254-260, July-Aug. 1978.

8 Hess, R. A., "Pursuit Tracking and Higher Levels of Skill Development in the Human Pilot”, IEEE Transactions on Systems, Man, and Cybernetics, Volume: 11, Issue: 4, April 1981.

9 Gaines, B., “Linear and Nonlinear Models of the Human Controller,” International Journal of Man-Machine Studies (1969) 1, 333-360.

10 Krendel, E. S., and McRuer, D. T., "A servomechanisms approach to skill development," J. Franklin Inst., vol. 269, pp. 24-42, Jan. 1960.

11 McRuer, D. T., A Neuromuscular Actuation System Model, IEEE Transactions on Man-Machine Systems, vol. MMS-9, no. 3, September 1968.

12 Hess, R. A., "A Rationale for Human Operator Pulsive Control Behavior,” Journal of Guidance, Control, and Dynamics, vol. 2, pp. 221-227, May-June 1979.

13 Hess, R. A., "Unified Theory for Aircraft Handling Qualities and Adverse Aircraft-Pilot Coupling", Journal of Guidance, Control, and Dynamics, Vol. 20, No. 6, 1997.

14 Roscoe, A. H., and Ellis, G. A., “A subjective rating scale assessing pilot workload in flight. A decade of practical use. Royal Aerospace Establishment.” Technical Report 90019. Farnborough. UK: Royal Aerospace Establishment, 1990.

15 Bachelder, E., and Aponso, B. “Novel Estimation of Pilot Performance Characteristics, AIAA Atmospheric Flight Mechanics Conference,” AIAA SciTech Forum, (AIAA 2017-1640).